Nucleating Pattern Formation in Spin-Coated Polymer Blend Films with Nanoscale Surface Templates

Joseph H. Wei,[†] David C. Coffey,[‡] and David S. Ginger*[,§]

Department of Chemical Engineering, University of Washington, Seattle, Washington 98195-1750, Department of Physics, University of Washington, Seattle, Washington 98195-1560, and Department of Chemistry, University of Washington, Seattle, Washington 98195-1700

Received: August 22, 2006; In Final Form: September 21, 2006

We use Dip-Pen Nanolithography (DPN) to generate monolayer surface templates for guiding pattern formation in spin-coated polymer blend films. We study template-directed pattern formation in blends of polystyrene/poly(2-vinylpyridine) (PS/P2VP) as well as blends of PS and the semiconducting conjugated polymer poly-(3-hexylthiophene) (P3HT). We show that acid-terminated monolayers can be used to template pattern formation in PS/P3HT blends, while hydrophobic monolayers can be used to template pattern formation in PS/P2VP blends. In both blends, the polymer patterns comprise laterally-phase separated regions surrounded by vertically separated bilayers. We hypothesize that the observed patterns are formed by template-induced dewetting of the bottom layer of a polymer bilayer during the spin-coating process. We compare the effects of template feature size and spacing on the resulting polymer patterns with predictions from published models of template-directed dewetting in thin films and find the data in good agreement. For both blends we observe that a minimum feature size is required to nucleate dewetting/phase separation. We find this minimum template diameter to be ∼180 nm in 50/50 PS/P2VP blends, and ∼100 nm in 50/50 PS/P3HT blends. For larger template diameters, PS/P2VP blends show evidence for pattern formation beginning at the template boundaries, while PS/P3HT blends rupture randomly across the template features.

Introduction

Demixing, dewetting, and pattern formation in thin polymer films are important to a range of applications including conventional lithographic resists,[1] antireflection coatings,[2] alternative nanofabrication strategies,[3−5] and conjugated-polymer-based optoelectronics.[6−20] In particular, much new interest in understanding and controlling the formation of nano- to microscale structure in polymer thin films is emerging due to the fact that film morphology can have a dramatic impact on both the electronic and the optical properties of semiconducting polymer transistors,[6−8] light-emitting diodes (LEDs),[9−11] and photovoltaics.[12−18]

Most conjugated polymer devices are formed by solution-processing methods such as spin-coating. The phase separation of polymer blends during spin-coating is a complicated kinetic process that can lead to nonequilibrium film structures that are sensitive to many experimental input parameters.[21,22] Nevertheless, this sensitivity can be exploited to control phase separation occurring in spin-coated films through the judicious choice of solvent, spin-coating speed, temperature, solvent atmosphere, and substrate surface chemistry. Patterned surface chemistry in particular has been studied as a means to control morphology and phase separation in both insulating and semiconducting polymer blends.[23−28] For instance, researchers in Cambridge have shown that microcontact-printed surface templates can improve light outcoupling in LEDs by inducing microscale periodicity in the lateral phase separation of conjugated polymer blend films processed from solution.[26,27] Despite such successes, and advances in the understanding of the kinetics of lateral phase separation during spin-coating,[21,22] the mechanism by which patterned surface chemistry guides the formation of final film morphologies in phase-separated blends remains an important open question. In addition, the template length scales probed experimentally to date have generally been in the range from 1 to 10 microns and larger,[23−27] while many interesting processes, particularly in conjugated polymers, occur on submicron or even sub-100 nm length scales.

To address these issues, and better understand the limits of resolution and accuracy with which nanoscale templates can guide phase separation, we recently described how Dip-Pen Nanolithography (DPN)[29] could be used to template polymer film morphology in blends of polystyrene (PS) and the semiconducting polymer poly(3-hexylthiophene) (P3HT), thereby producing semiconducting polymer features as small as ∼150 nm using surface templates as small as ∼50 nm in diameter.[28] In the present paper, we use the unique abilities of DPN to study surface-templated lateral phase separation in spin-coated polymer blend films. We go beyond proof-of-principle to make a systematic study of the impact of surface chemistry, template size, and template spacing on pattern formation in model blends of polystyrene (PS) and poly(2-vinylpyridine) (P2VP). We study pattern formation induced by templates on the submicron down to sub-100 nm length scales, providing data that has previously been difficult to obtain. We demonstrate the capability to nucleate individual, size-controlled domains of PS in PS/P2VP and contrast the resulting polymer patterns with an extensive data set from the PS/P3HT system. We use these data to make a comparison with models of pattern formation in polymer thin films via template-directed dewetting.[30−36] The data on these

* Corresponding author. Phone: (206) 685-2331. Fax: (206) 685-8665. E-mail: ginger@chem.washington.edu.
[†] Department of Chemical Engineering.
[‡] Department of Physics.
[§] Department of Chemistry.

10.1021/jp065409a CCC: $33.50
Published on Web 11/11/2006

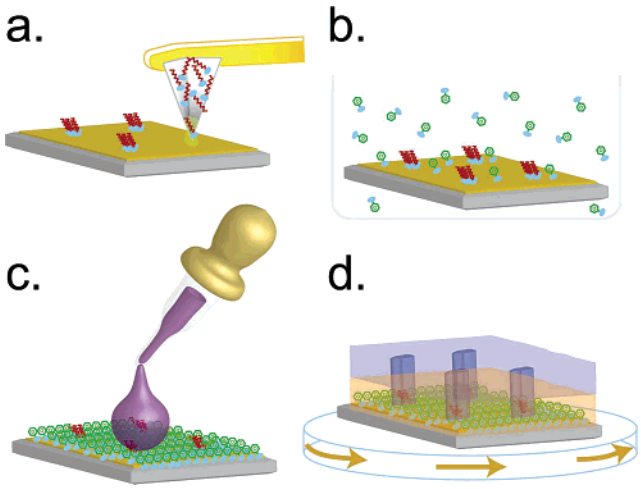

Figure 1. Experimental schematic. (a) Dip-Pen Nanolithography (DPN) is used to generate templates comprising patterned self-assembled monolayers of alkanethiols (1-octadecanethiol "ODT" or 16-mercaptohexadecanoic acid "MHA") on gold-coated silicon substrates. (b) Unpatterned regions of the gold surface are backfilled with benzenethiol. (c) A polymer blend is spin-coated from a common solvent onto the patterned surface. (d) By the time the solvent evaporates, the polymer film has adopted a structure that reflects the underlying template.

blends are in good qualitative agreement with the published models of dewetting single-component films, and we conclude that pattern formation in polymer blends (at least under the studied conditions) occurs via template-nucleated dewetting of the bottom layer of a transient vertically phase-separated fluid bilayer[22] during the spin-coating process.

Experimental Methods

Figure 1 depicts our experimental approach, the details of which have been described elsewhere.[28] Briefly, we use DPN to generate high-resolution patterned alkanethiol monolayers on gold substrates, which are then backfilled with a second thiol from solution. A blend of two polymers in a common solvent is then spin-coated onto the patterned substrate. In many cases the template guides the phase separation process during spin-coating, and the resulting films are subsequently studied by scanning probe microscopy and other surface sensitive techniques.

For this study, PS (M_w: 95 500, M_n: 91 000, M_w/M_n: 1.05, Polymer Source, Inc.) and P2VP (M_w: 159 000, M_n: 152 000, M_w/M_n: 1.05, Aldrich Chemical Corporation) were chosen as model polymers to compare with the PS/P3HT system due to the extensive literature available on PS and P2VP thin film properties. We contrast the phase separation of this system with that of PS (M_w: 110 000, Aldrich Chemical Corporation) and P3HT (M_w: 55 000, M_n: 22 800, American Dye Source), as an example of another easily characterized model blend (the PS/P3HT system exhibits optical, electrical, and elemental contrast).

To prepare substrates for DPN, a Si wafer was diced and then immediately blown with a dry nitrogen stream to remove visible silicon dust. Prior to metal deposition, the substrates were further cleaned by sonication in acetone for 25 min and then in isopropyl alcohol for 25 min. Gold films were deposited by thermal evaporation (Auto 306, Edwards) of 45 nm of Au (from 99.999% pellets, K. J. Lesker) onto a 4.5 nm chromium adhesion layer (from chromium-coated tungsten rods, Midwest Tungsten Service) on thermally oxidized Si wafers (10 000 Å ± 5% thermal oxide, <1-0-0>, Silicon Quest International). The metals were deposited by thermal evaporation at ~1 Å/s, and the substrates were used for DPN within 2 days of metal deposition.

DPN has been described extensively in other publications,[29,37−39] and we summarize only the most relevant details here. DPN tips for writing 1-octadecanethiol (ODT) were prepared by coating silicon nitride probes (DPN Probes, type A, NanoInk, Inc.) with ODT (98%, Aldrich Chemical Corporation) via thermal evaporation at ~60 °C by sealing a probe for 25 min in a metal canister using a temperature controlled heater block (VWR) and then allowing it to cool to room temperature before use.

DPN tips for writing 16-mercaptohexadecanoic acid (MHA) were prepared by dipping silicon nitride probes in a saturated solution of MHA (90%, Aldrich Chemical Corporation) in acetonitrile (HPLC grade, Fisher Scientific) for 5 s. The tips were then exposed to water vapor for 5 min before being dipped in the MHA/acetonitrile solution again for 15 s and subsequently blown dry with compressed gas (Dust Off, Falcon).

Surface patterning was performed using either a NanoInk Nscriptor or an Asylum MFP-3D scanning probe microscope in ambient atmosphere (temperature typically 21−24 °C, relative humidity typically 30−40%). After patterning with DPN, the unpatterned areas of the substrates were coated with a layer of benzenethiol by immersion in a 1 mM benzenethiol (99%, Aldrich Chemical Corporation) solution in ethanol (AAPER Alcohol and Chemical Corporation) for ~1 min. At these times negligible place-exchange of the DPN-patterned thiols by the solution-deposited thiols is anticipated.[40,41] In experiments involving backfilling with other thiols (Supporting Information), the thiols were all prepared as 1 mM solutions in ethanol.

The PS/P2VP polymer films (~30 nm final thickness) were prepared by spin-coating from 1% (w/w) chlorobenzene solutions onto the thiol-coated gold substrates with a liquid spreading pre-spin at 300 rpm for 3 s, followed by a coating spin at 2400 rpm for 32 s (WS-400B-6NPP/LITE from Laurell Technologies Corporation) using the maximum acceleration setting of 21 675 rpm/s. PS/P3HT films were prepared by spin-coating at 2000 rpm for 30 s at maximum acceleration (set at 21 675 rpm/sec) also from chlorobenzene solution (1 w/v %). All solutions were filtered through 0.45 μm PTFE membranes (HPLC certified acrodisc CR 13 mm syringe filter from Pall Life Sciences) before spin-coating.

The resulting polymer films were imaged with both NanoInk Nscriptor and/or Asylum MFP-3D scanning probe microscopes. Selective etching of the polymers[23] was performed by dissolving the films in either cyclohexane or ethanol for 1−5 min. X-ray photoelectron spectroscopy (XPS) (Surface Science Instruments x-probe spectrometer) was used to determine the surface elemental compositions (Supporting Information).

Results and Discussion

We screened a variety of template and backfill chemistries with both DPN and microcontact-printed templates and tested ODT and MHA templates with backfills of benzenethiol, 11-mercapto-1-undecanol, MHA, and 6-amino-1-hexanethiol (hydrochloride salt). Only the combination of an ODT template with a benzenethiol background exhibited reliable pattern formation in spin-coated PS/P2VP films (Supporting Information). For the PS/P3HT system, ODT templates with benzenthiol backgrounds also led to pattern formation (Supporting Information), but MHA templates were more uniform and reproducible. Thus, for the body of this paper we focus on studying ODT templates with PS/P2VP films, and MHA templates with PS/

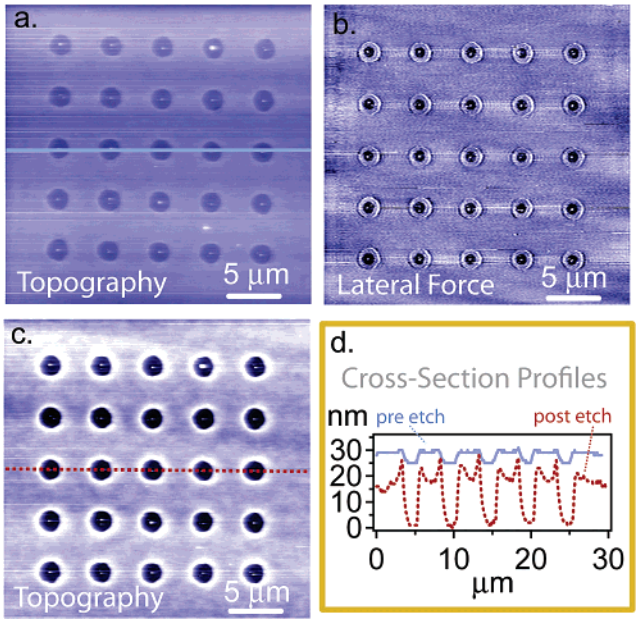

Figure 2. Morphology of PS/P2VP blends spin-coated onto DPN templates. (a) Contact-mode AFM topography image of a PS/P2VP (50/50) blend spin-coated onto a DPN-generated ODT template (*z*-range: 40 nm). (b) AFM lateral force (friction) image of the film in Figure 2a following etching in cyclohexane to dissolve the PS. The low friction (black) dots are the exposed ODT templates. (c) AFM topography of the same region (*z*-range: 40 nm). (d) Cross-sectional height profiles of films from Figure 2a (before etching) (blue line) and Figure 2c (after etching) (red line) showing the increase in hole depth upon etching.

P3HT films. We note that the templates that lead to the most successful patterning (ODT and MHA) represent cases of strong contrast in surface chemistry (the most hydrophobic and most hydrophilic templates studied) consistent with the pattern formation mechanism based on surface energy gradients discussed below.

Figure 2a shows a contact-mode atomic force microscope (AFM) image of a typical polymer pattern formed from a 50/50 PS/P2VP blend spin-coated onto a hydrophobic ODT template with a benzenethiol-coated background. Clear indication of the template influence on the film structure is seen in the topography image, although the line trace (Figure 2d, blue solid line) shows that the variation in topography across the patterns is only 5 nm, or ~15% of the total 31 nm film thickness. To better understand this structure, we obtain more detailed information about the film by etching the film with cyclohexane, which dissolves PS but not P2VP.

Figure 2b (lateral force) and Figure 2c (topography) show the film from Figure 2a after etching with cyclohexane, and the red dashed line in Figure 2d indicates the corresponding cross-sectional profile. The cyclohexane etch removes the top PS film (decreasing the film thickness to 16 nm) and leaves behind a P2VP film with holes centered on the ODT template dots. These holes completely penetrate the P2VP layer, and the ODT template which initiated the pattern formation is visible in the lateral force image of the etched film (Figure 2b). In the absence of an ODT template a 50/50 PS/P2VP blend spin-coated onto a benzethiol layer produces a bilayer film with a PS layer on top and a buried P2VP layer, as verified by both XPS and selective etching experiments (Supporting Information).

Figure 3a shows the final morphology of the patterned PS/P2VP films as deduced from the AFM, XPS, and etching data. It comprises a top layer of PS which penetrates an underlying

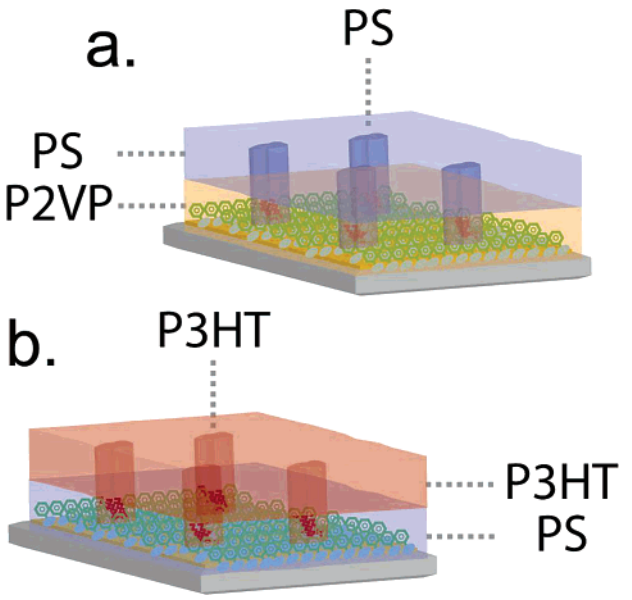

Figure 3. Schematic depiction of final film morphology. (a) PS/P2VP film structure on an ODT template. (b) PS/P3HT film structure on an MHA template. (PS = blue; P2VP = orange; P3HT = red).

layer of P2VP in regions dictated by the DPN-generated surface template. The final structure of these PS/P2VP patterns formed on the hydrophobic ODT templates is thus remarkably similar to the morphology obtained with PS/P3HT films spin-coated onto polar MHA templates (Figure 3b),[28] except of course that in the latter instance the PS forms the bottom layer and the P3HT forms the columns. The strong similarity in film morphology shared between the systems suggests that a common mechanism of film formation might be at work.

In both the PS/P2VP and PS/P3HT systems, we find that the observed structures are formed during the spin-coating process. Although the generated morphologies may be metastable,[21] we have not observed changes in film morphology over times from a few hours to a few months after spin-coating. Furthermore, we have annealed the samples at 108 °C for 24 h without any significant change in film structure. However, annealing at higher temperatures (above 115 °C) ultimately leads to dewetting of the entire film. We note that the bulk glass transition temperature, T_g, for the PS, M_w: 12.0−117 kDa, is reported in the range of ~95−100 °C,[42−45] while for P2VP, M_w: 8.1−60 kDa, T_g is reported as ~95−104 °C.[44−46] We also note that the bulk T_g is known to be altered in thin films[42] and is affected by surface chemistry.[1] The absence of significant film evolution after spin-coating is in contrast to some studies on single component films on patterned surfaces.[47] We thus consider possible mechanisms through which the polymer pattern formation could occur during the spin-coating process before the solvent has evaporated.

Walheim et al. proposed,[21] and Heriot and Jones experimentally verified,[22] that some polymer blend systems form a transient bilayer due to preferential wetting of the substrate by one polymer/solvent phase during spin-coating. In that case, any lateral phase separation results from an instability developing in the interface between the vertically stratified liquid layers when the drying film reaches some critical thickness or when the film develops a large solvent concentration gradient in the direction perpendicular to the film surface. Certainly our experimental observations are consistent with the transient bilayer hypothesis: in the absence of any DPN templates, we observe that both PS/P2VP and PS/P3HT films form vertically separated bilayers under the range of studied conditions.

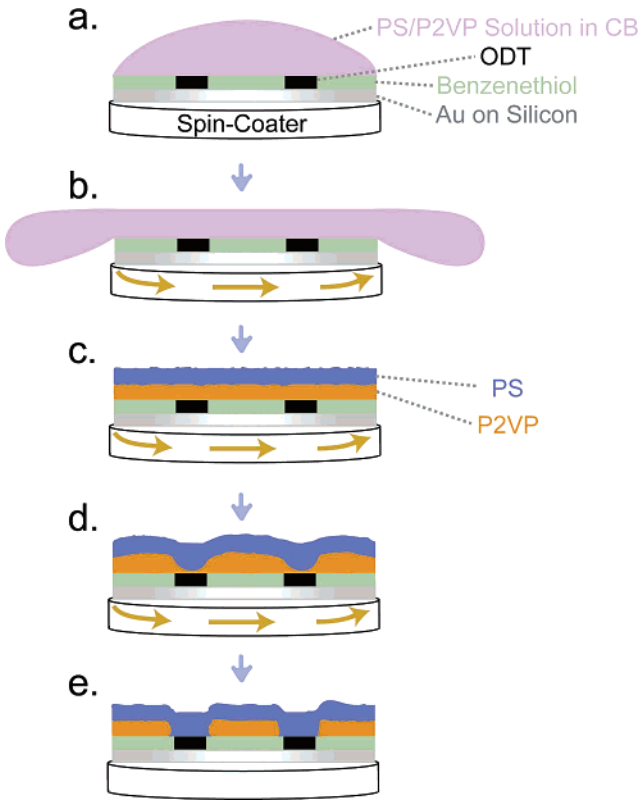

Figure 4. Proposed templating process. (a) A PS/P2VP blend dissolved in chlorobenzene (CB) is dropped onto a DPN-generated surface template. (b) Excess solvent/polymer is lost during initial spin-up. (c) Transient liquid−liquid bilayer structure forms. (d) The film thins, the bottom polymer layer dewets from surface template; the top layer flows into the dewetted hole. (e) The solvent evaporates and the film vitrifies, locking in laterally phase-separated structures in a vertically phase-separated background.

However, one question left open by this hypothesis is the means by which patterned substrate chemistry influences the final film structure.

We believe a plausible hypothesis to explain the final morphologies observed in the films studied herein is found in the work of Sharma and co-workers[30−36] describing pattern formation in thin polymer films by template-directed dewetting. In their hydrodynamic model, film/substrate interactions are described by a position dependent potential, parametrized to include both long-range van der Waals and short-range intermolecular interactions.[30] Dewetting then occurs by fluid flow from the less wettable to more wettable regions of a substrate as induced by the substrate potential gradient.[30] The potential gradient which leads to dewetting can result from either local surface chemistry, or local topography. However chemical contrast is predicted to dominate over topographic contrast,[30] and we believe chemical contrast is the factor responsible for the dewetting observed in this study. Changes in surface topography due to the different monolayers are relatively insignificant, as we are modifying the gold substrates (RMS roughness: 0.6 ± 0.1 nm) with monolayers that are at most 2.2 nm thick,[48] and we observe successful pattern formation in films which range in final thickness from less than 30 to more than 80 nm thick. In addition, if changes in surface topography were the primary cause of the dewetting, templates with similar thicknesses (e.g. ODT and MHA) should cause similar patterning behavior. Since MHA and ODT templates behave quite differently (MHA templates do not cause pattern formation in PS/P2VP blends while ODT templates do), we conclude that contrast in surface chemistry, rather than surface topography, is responsible for the observed dewetting patterns.

Although the models of Sharma and co-workers consider single-component films, nucleated dewetting of the bottom layer of a vertically separated polymer/solvent film (accompanied by fluid flow of the top liquid layer into the hole) would produce patterns consisting of holes in an underlying polymer film filled with the material from the overlying polymer layer. This hypothesis is depicted schematically in Figure 4. Significantly, however, we do *not* observe pattern formation using single-component polymer films on the DPN templates, even after thermal annealing for our studied film/template chemistry combinations. This could be expected if, for instance, the polymer/air interface is higher in energy than the polymer/polymer interface.

While this nucleated dewetting hypothesis seems satisfactory in describing the observed final film structures, the flexibility of DPN to generate a variety of template sizes and shapes allows us to compare our patterning results with the predictions from the model of Sharma et al. in more detail. As one example, it has been predicted[33] that as the size of a less-wettable surface patch in a more-wettable background is increased, the dewetting

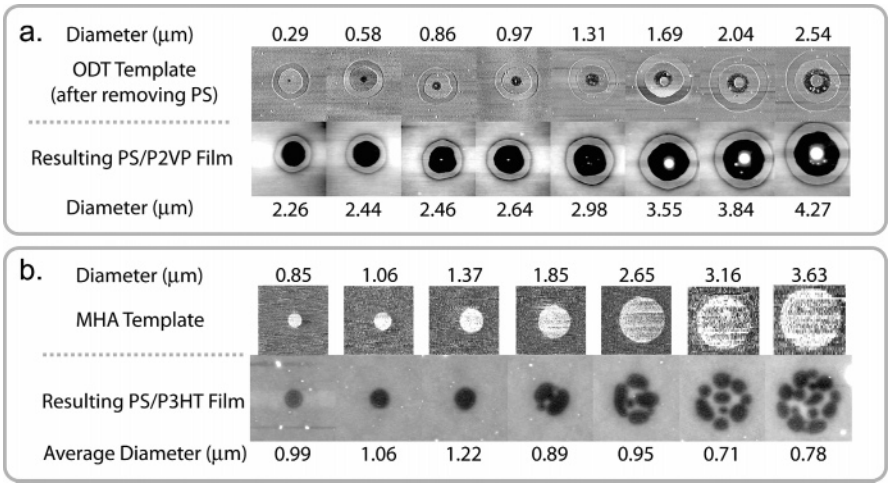

Figure 5. Evolution of film morphology with template size for PS/P2VP and PS/P3HT blends. (a) Lateral force images (top: after cyclohexane etching) and AFM topography (bottom: before cyclohexane etching) of a 50/50 PS/P2VP blend on ODT templates of various diameters. (b) Lateral force images (top: before spin-coating) and AFM topography (bottom: after spin-coating) of a 50/50 PS/P3HT blend on MHA templates of various diameters.

rate, driven by the gradient in surface energies, will be highest at the boundary between the regions of different surface chemistry.

Figure 5 shows the effect of template size on morphology and final size of the nucleated domains for both the PS/P2VP (Figure 5a) and PS/P3HT (Figure 5b) systems. For the PS/P2VP blends, we observe that the size of the final nucleated PS domain increases as the ODT template size is increased. However, above a certain size (~860 nm), P2VP droplets start to form at the centers of the PS domains. In addition, we observed an elevated rim surrounding the hole in the P2VP layers in Figure 5a. We attribute these rims to the buildup of the displaced P2VP layer. However, we note that not all samples show such pronounced rims, even for comparable template diameters and polymer feature sizes (Supporting Information). In the PS/P3HT blends (Figure 5b), at small template sizes only single P3HT domains are formed, centered on the MHA monolayer templates. However, as the template is enlarged (~1.6 μm), the single laterally-separated domains begin to rupture into multiple domains, suggesting that dewetting of the bottom polymer layer is occurring rapidly across the MHA template. Indeed, on samples backfilled with MHA, similar phase separation occurs everywhere on the substrate.

Figure 6 compares the final size of the nucleated polymer features with the size of the underlying template in more detail. In Figure 6a, we see that the outer diameter of the PS domains formed in the PS/P2VP blends track linearly with the size of the templates over the entire range studied (from ~180 nm to ~6 μm). However, above a certain template diameter the PS domains contain secondary droplets of "trapped" P2VP near the template centers. The observation of trapped P2VP droplets in the PS domains (as seen in Figure 5a) is consistent with a transition from dewetting from the template centers, to dewetting dominated by the template edges as predicted by Kargupta and Sharma[33] and previously observed by Sehgal et al.[47] during the dewetting of single-component polymer films. We assign the transition diameter, $D_t \sim 1.1 \pm 0.3$ μm (mean $\pm$ standard deviation for a series of 23 different patterns), to be the template diameter at which we first observe P2VP droplets within the PS domain that remain attached to the substrate after cyclohexane etching.

In Figure 6a, while the final polymer feature size tracks the template size with a similar slope across all samples, the offset (corresponding to the distance a hole has grown past the edge of the template) varies from sample to sample. We hypothesize that this varying offset results from different degrees of quality and cleanliness of the background benzenethiol layer, which therefore provide different degrees of wettability to the polymer film. One potential source of variability could be inadvertent ODT contamination of the substrate: during DPN with freshly coated ODT tips, it is known that a small amount of ODT can be deposited by vapor transport to the unpatterned areas of the substrate (an effect which is sensitive to the tip and substrate temperature and length of patterning). Consistent with this hypothesis, when we intentionally backfilled substrates with mixtures of benzenthiol and various amounts of hexanethiol from solution, we found that backfilling with higher relative concentrations of hexanethiol led to faster dewetting and larger "offsets" (Supporting Information).

Figure 6b shows a similar plot of polymer feature diameter versus monolayer template diameter for the PS/P3HT blend. However, in the PS/P3HT system we do not observe a transition from center-dominated to edge-dominated dewetting as the template diameter is increased (Figure 6b inset). Instead, once

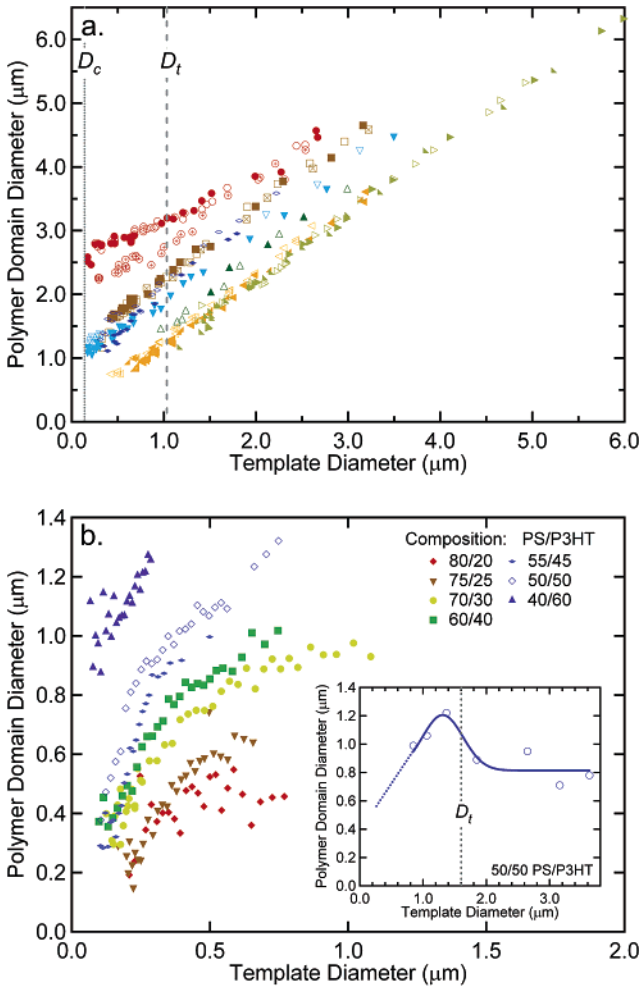

Figure 6. Polymer domain size as a function of template size. (a) Nucleated PS domain diameter plotted versus ODT template size for 18 different patterns (plotted as different symbols) on seven different substrates (plotted as different colors). As discussed in the text, the D_c and D_t lines indicate, respectively, the minimum template diameter at which nucleation is observed, and the threshold diameter at which nucleation begins to proceed from the template boundary rather than the template center. (b) Nucleated P3HT domain diameter plotted as a function of template diameter for a series of different PS/P3HT blend ratios (as indicated in figure). (b inset) Same plot for the 50/50 PS/P3HT blend at larger template diameters. As discussed in the text, D_t indicates the template size at which multiple P3HT domains form on a single template.

the template is larger than a given diameter, D_t (~1.6 μm in the 50/50 PS/P3HT), the single P3HT domain ruptures into multiple domains of varying size (Figure 5b), suggesting that dewetting/phase separation is occurring rapidly across the entire template, and that multiple domains could be forming faster than a single domain can grow to occupy the entire template. Figure 6b plots the polymer domain size for templates smaller than D_t in various blend compositions. It appears to show a change in slope in the plot of P3HT domain size versus template diameter for the PS/P3HT blends. This change in slope is not an intrinsic property of the individual templates, but rather results from coupling between template dots when the pitch (center-to-center distance between dots) is comparable to the final feature size. This effect is shown more clearly in Figure 7, which shows how, for identical template diameters, the final polymer feature size decreases with the pitch until eventually the dots begin to merge. Similar behavior has again been qualitatively predicted[33] and observed for dewetting PS films from linear stripes.[47] In contrast, however, the domain sizes in

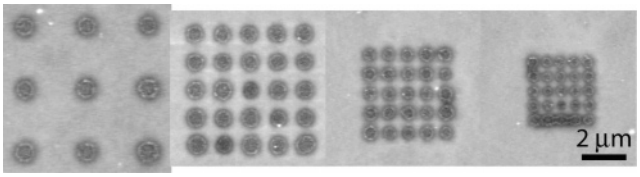

Figure 7. Effect of template pitch on polymer feature size. AFM topography images of PS/P3HT blends (50/50) showing that the polymer feature diameter decreases as the template pitch size decreases until the domains begin to merge, even when the underlying MHA template diameter, 400 nm, is kept constant.

the PS/P2VP blends do not shrink as significantly as the pitch distance decreases until the domains begin to merge (Supporting Information).

Finally, we examine the probability of nucleating a polymer domain as a function of the template diameter. Kargupta and Sharma have predicted a minimum critical size, D_c, associated with the smallest heterogeneous surface patch which can successfully nucleate dewetting of the polymer film and predicted that D_c can be much smaller (by at least an order of magnitude) than λ, the wavelength associated with spinodal dewetting of the film from a homogeneous substrate.[33,36] Figure 8 plots the probability that a polymer feature is nucleated on top of a surface template patch for both PS/P2VP (Figure 8a) and PS/P3HT blends (Figure 8b) as a function of template diameter. Both polymers show reliable nucleation for feature sizes well below 1 μm. The nucleation probability in the 50/50 PS/P2VP blends falls to 50% for ODT templates of ~300 nm in diameter, dropping to zero as the ODT templates are reduced below ~180 nm in diameter. For the 50/50 PS/P3HT blend the nucleation rate falls to 50% for template diameters of ~120 nm and decreases to zero at ~100 nm. From the above, we assign D_c as ~180 nm for PS/P2VP (50/50) and D_c as ~100 nm for PS/P3HT (50/50). These values of D_c are indeed significantly smaller than typical length scales associated with spinodal dewetting of thin polymer films. The comparatively small values we observe for D_c emphasize the impact that nanoscale surface heterogeneities can have on thin film structures. Finally, in Figure 8b we also investigate the dependence of D_c on film composition and find that films with higher P3HT weight fractions nucleate P3HT domains more readily than do films with lower P3HT weight fractions. This can be understood because, at constant weight fraction of polymer in solution, increasing the P3HT composition corresponds to decreasing the PS content and hence decreasing the thickness of the bottom PS layer.

Conclusions

We have shown that nano- and microscale surface templates generated with DPN can be used to guide pattern formation in spin-coated blends of PS/P2VP and PS/P3HT and have used the unique experimental flexibility afforded by DPN to generate templates to study systematically the effect of nanoscale surface templates on pattern formation in spin-coated polymer blends. Under the range of conditions studied, we have shown that blends of PS/P2VP form vertically separated bilayers with the P2VP layer in contact with the benzenethiol-coated gold, while PS/P3HT blends form vertically separated bilayers with the PS in contact with the benzenethiol-coated gold. Nanoscale ODT templates were shown to lead to reliable site-specific pattern formation in spin-coated PS/P2VP blends, while nanoscale MHA templates were shown to lead to reliable site-specific pattern formation in spin-coated PS/P3HT blends. Significantly, we have shown that in both blend systems the final film structure

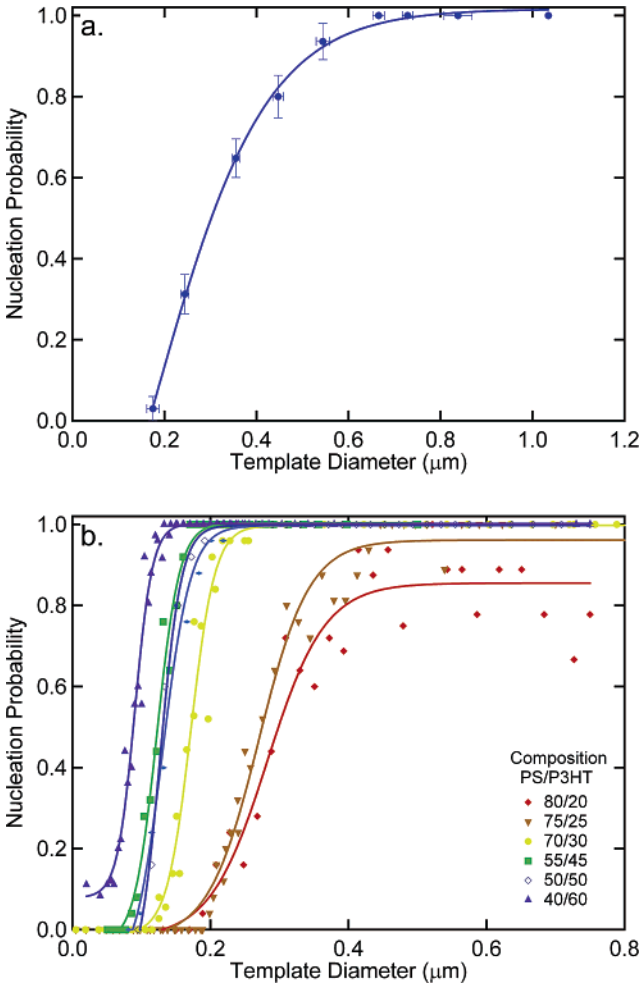

Figure 8. Nucleation probability as a function of template size. (a) The nucleation probability in the PS/P2VP blends (50/50) determined from arrays of 25 dots, binned by template diameter. (Error bars represent the standard deviation of the mean nucleation probability across multiple 25 dot arrays binned by template diameter). (b) The nucleation probability versus template diameter for PS/P3HT blends of different PS/P3HT ratios (as indicated on the plot).

is consistent with a mechanism of pattern formation by nucleated dewetting of the bottom polymer layer at the DPN-generated surface heterogeneities. We compared the effects of template size and spacing on the final film structure with qualitative predictions from models of nucleated dewetting in thin single-component films, and we found generally good agreement with the patterns formed in the polymer blends. For both blends, the nucleation rate of laterally phase-separated features increases with the size of the surface heterogeneity, and no nucleation is observed below a critical template size, D_c (~180 nm for 50/50 PS/P2VP and ~100 nm for 50/50 PS/P3HT). In addition, as the template diameter is increased (D_t: ~1.1 μm for 50/50 PS/P2VP and ~1.6 μm for 50/50 PS/P3HT), multiple polymer features are nucleated at each template dot. Although the final film structures and pattern formation mechanisms appear very similar, differences between the two blend systems are also observed. For PS/P2VP blends on ODT templates larger than the threshold diameter, D_t, the dewetting appears to occur from the template edges, leading to trapped P2VP droplets at the center of the template. In contrast, for PS/P3HT blends on MHA templates larger than D_t, multiple randomly oriented droplets are formed within the template.

With the growth of polymer-based optoelectronics, controlling film morphology and pattern formation in solution-processed

polymer blends on the nanometer-to-micrometer scale is becoming increasingly important. The results presented above, which would have been extremely difficult to obtain with more conventional experimental methods such as microcontact printing, provide evidence that dewetting of transient multilayers is one specific mechanism through which surface chemistry can be used to exert control over the morphology of polymer blend films processed from solution. DPN provides a powerful tool to investigate these effects for a range of feature sizes and surface chemistries.

Acknowledgment. This paper is based in part on work supported by the University of Washington, the National Science Foundation (DMR 0449422 and DMR 0120967), and the Air Force Office of Scientific Research (FA9550-05-1-0467 and FA9550-05-1-0231). The XPS data were obtained at the National ESCA and Surface Analysis Center for Biomedical Problems, supported by NIBIB grant EB-002027.

Supporting Information Available: XPS surface elemental compositions of PS surface, P2VP surface, and PS/P2VP blend film; total film thickness before and after cyclohexane etching in different blends of PS/P2VP; evolution of film morphology with template size for PS/P2VP films for which the rim feature is not observed; AFM topography image of a PS/P2VP blend spin-coated onto a DPN-generated MHA template with benzenethiol background on gold; AFM topography of pattern formation in PS/P2VP films with ODT templates (both DPN-generated and microcontact-printed) in various background chemistry; AFM topography of pattern formation in PS/P3HT films with ODT templates; dependence of the dewetting rate on various amounts of hexanethiol with benzenethiol on the unpatterned region of the substrate; AFM lateral force images of PS/P2VP film structure with different pitch sizes after cyclohexane etching. This material is available free of charge via the Internet at http://pubs.acs.org.

References and Notes

(1) D'Amour, J. N.; Okoroanyanwu, U.; Frank, C. W. *Microelectron. Eng.* **2004**, *73*−*74*, 209.
(2) Walheim, S.; Schaffer, E.; Mlynek, J.; Steiner, U. *Science* **1999**, *283*, 520.
(3) Aizawa, M.; Buriak, J. M. *J. Am. Chem. Soc.* **2005**, *127*, 8932.
(4) Wang, Y.; Liu, Z. M.; Han, B. X.; Sun, Z. Y.; Zhang, J. L.; Sun, D. H. *Adv. Funct. Mater.* **2005**, *15*, 655.
(5) Misner, M. J.; Skaff, H.; Emrick, T.; Russell, T. P. *Adv. Mater.* **2003**, *15*, 221.
(6) Yang, H. C.; Shin, T. J.; Yang, L.; Cho, K.; Ryu, C. Y.; Bao, Z. N. *Adv. Funct. Mater.* **2005**, *15*, 671.
(7) Stingelin-Stutzmann, N.; Smits, E.; Wondergem, H.; Tanase, C.; Blom, P.; Smith, P.; De Leeuw, D. *Nat. Mater.* **2005**, *4*, 601.
(8) Kline, R. J.; McGehee, M. D.; Toney, M. F. *Nat. Mater.* **2006**, *5*, 222.
(9) Morteani, A. C.; Sreearunothai, P.; Herz, L. M.; Friend, R. H.; Silva, C. *Phys. Rev. Lett.* **2004**, *92*, 247402.
(10) Morteani, A. C.; Dhoot, A. S.; Kim, J. S.; Silva, C.; Greenham, N. C.; Murphy, C.; Moons, E.; Cina, S.; Burroughes, J. H.; Friend, R. H. *Adv. Mater.* **2003**, *15*, 1708.
(11) Wenzl, F. P.; Pachler, P.; Suess, C.; Haase, A.; List, E. J. W.; Poelt, P.; Somitsch, D.; Knoll, P.; Scherf, U.; Leising, G. *Adv. Funct. Mater.* **2004**, *14*, 441.
(12) Halls, J. J. M.; Arias, A. C.; MacKenzie, J. D.; Wu, W. S.; Inbasekaran, M.; Woo, E. P.; Friend, R. H. *Adv. Mater.* **2000**, *12*, 498.
(13) Arias, A. C.; MacKenzie, J. D.; Stevenson, R.; Halls, J. J. M.; Inbasekaran, M.; Woo, E. P.; Richards, D.; Friend, R. H. *Macromolecules* **2001**, *34*, 6005.
(14) Moons, E. *J. Phys.: Condens. Matter* **2002**, *14*, 12235.
(15) McNeill, C. R.; Dastoor, P. C. *J. Appl. Phys.* **2006**, *99*, 033502.
(16) Hoppe, H.; Niggemann, M.; Winder, C.; Kraut, J.; Hiesgen, R.; Hinsch, A.; Meissner, D.; Sariciftci, N. S. *Adv. Funct. Mater.* **2004**, *14*, 1005.
(17) van Duren, J. K. J.; Yang, X. N.; Loos, J.; Bulle-Lieuwma, C. W. T.; Sieval, A. B.; Hummelen, J. C.; Janssen, R. A. J. *Adv. Funct. Mater.* **2004**, *14*, 425.
(18) Coffey, D. C.; Ginger, D. S. *Nat. Mater.* **2006**, *5*, 735.
(19) Schwartz, B. J. *Annu. Rev. Phys. Chem.* **2003**, *54*, 141.
(20) Chappell, J.; Lidzey, D. G.; Jukes, P. C.; Higgins, A. M.; Thompson, R. L.; O'Connor, S.; Grizzi, I.; Fletcher, R.; O'Brien, J.; Geoghegan, M.; Jones, R. A. L. *Nat. Mater.* **2003**, *2*, 616.
(21) Walheim, S.; Boltau, M.; Mlynek, J.; Krausch, G.; Steiner, U. *Macromolecules* **1997**, *30*, 4995.
(22) Heriot, S. Y.; Jones, R. A. L. *Nat. Mater.* **2005**, *4*, 782.
(23) Boltau, M.; Walheim, S.; Mlynek, J.; Krausch, G.; Steiner, U. *Nature* **1998**, *391*, 877.
(24) Karim, A.; Douglas, J. F.; Lee, B. P.; Glotzer, S. C.; Rogers, J. A.; Jackman, R. J.; Amis, E. J.; Whitesides, G. M. *Phys. Rev. E* **1998**, *57*, R6273.
(25) Raczkowska, J.; Cyganik, P.; Budkowski, A.; Bernasik, A.; Rysz, J.; Raptis, I.; Czuba, P.; Kowalski, K. *Macromolecules* **2005**, *38*, 8486.
(26) Corcoran, N.; Ho, P. K. H.; Arias, A. C.; Mackenzie, J. D.; Friend, R. H.; Fichet, G.; Huck, W. T. S. *Appl. Phys. Lett.* **2004**, *85*, 2965.
(27) Fichet, G.; Corcoran, N.; Ho, P. K. H.; Arias, A. C.; MacKenzie, J. D.; Huck, W. T. S.; Friend, R. H. *Adv. Mater.* **2004**, *16*, 1908.
(28) Coffey, D. C.; Ginger, D. S. *J. Am. Chem. Soc.* **2005**, *127*, 4564.
(29) Ginger, D. S.; Zhang, H.; Mirkin, C. A. *Angew. Chem., Int. Ed.* **2004**, *43*, 30.
(30) Kargupta, K.; Sharma, A. *Langmuir* **2002**, *18*, 1893.
(31) Kargupta, K.; Konnur, R.; Sharma, A. *Langmuir* **2000**, *16*, 10243.
(32) Kargupta, K.; Konnur, R.; Sharma, A. *Langmuir* **2001**, *17*, 1294.
(33) Kargupta, K.; Sharma, A. *Phys. Rev. Lett.* **2001**, *86*, 4536.
(34) Kargupta, K.; Sharma, A. *J. Colloid Interface Sci.* **2002**, *245*, 99.
(35) Kargupta, K.; Sharma, A. *Langmuir* **2003**, *19*, 5153.
(36) Konnur, R.; Kargupta, K.; Sharma, A. *Phys. Rev. Lett.* **2000**, *84*, 931.
(37) Piner, R. D.; Zhu, J.; Xu, F.; Hong, S. H.; Mirkin, C. A. *Science* **1999**, *283*, 661.
(38) Yu, M.; Nyamjav, D.; Ivanisevic, A. *J. Mater. Chem.* **2005**, *15*, 649.
(39) Im, J.; Huang, L.; Kang, J.; Lee, M.; Lee, D. J.; Rao, S. G.; Lee, N. K.; Hong, S. *J. Chem. Phys.* **2006**, *124*, 224707.
(40) Schlenoff, J. B.; Li, M.; Ly, H. *J. Am. Chem. Soc.* **1995**, *117*, 12528.
(41) Hostetler, M. J.; Templeton, A. C.; Murray, R. W. *Langmuir* **1999**, *15*, 3782.
(42) Sills, S.; Overney, R. M.; Chau, W.; Lee, V. Y.; Miller, R. D.; Frommer, J. *J. Chem. Phys.* **2004**, *120*, 5334.
(43) Kim, J. K.; Son, H. W.; Lee, Y. B.; Kim, J. W. *J. Polym. Sci., Part B: Polym. Phys.* **1999**, *37*, 889.
(44) van Krevelen, D. W. *Properties of Polymers*; 3rd ed.; Elsevier Scientific Publishing Company Inc.: Amsterdam, The Netherlands, 1990.
(45) Kang, H. M.; Lee, S. H.; Kim, S.; Char, K. *Macromolecules* **2003**, *36*, 8579.
(46) Gan, Y. D.; Zoller, J.; Yin, R.; Hogenesch, T. E. *Macromol. Symp.* **1994**, *77*, 93.
(47) Sehgal, A.; Ferreiro, V.; Douglas, J. F.; Amis, E. J.; Karim, A. *Langmuir* **2002**, *18*, 7041.
(48) Bain, C. D.; Troughton, E. B.; Tao, Y. T.; Evall, J.; Whitesides, G. M.; Nuzzo, R. G. *J. Am. Chem.* Soc. **1989**, *111*, 321.